Electronic Structure and Reactivity of TM-Doped La₁₋ₓSrₓCoO₃ (TM=Ni, Fe) Heterogeneous Catalysts

S C Grice[1], W R Flavell[1*], A G Thomas[1], S Warren[1], P G D Marr[1], D E Jewitt[1], N Khan[1], P M Dunwoody[1] and S A Jones[2]**

[1]Department of Physics, UMIST, PO Box 88, Manchester M60 1QD, UK

[2] Synetix, PO Box 1, Belasis Avenue, Billingham, Cleveland, TS23 1LB, UK

Tel.: (+44 (0) 161 200 4466, Fax: +44 (0) 161 200 3941, E-mail: wendy.flavell@UMIST.ac.uk

URL: http://chemist.phy.umist.ac.uk/

*Author to whom correspondence should be addressed.

** Current address: ESRF, BP 2200, F-38043, Grenoble, France

Abstract: The catalytic properties of LaCoO₃ in aqueous oxidation are explored as a function of doping. Both Sr substitution for La and Fe/Ni substitution for Co are studied. The reaction of interest is the aqueous epoxidation of crotyl alcohol with hydrogen peroxide. The reaction products are measured using GC, and the decomposition of hydrogen peroxide is studied using the volume of oxygen evolved during reaction. Strong variations in the activity to epoxide formation are observed, with Fe-doped samples being rather inactive in the reaction. SR VUV photoemission is used to explore the surface reactivity of the ceramic catalysts in aqueous solution, using H₂O as a probe molecule. These measurements are complemented by XANES measurements designed to probe the local defect structure and XPS measurements of surface composition. We relate the observed catalytic activity to the defect structure of the doped materials. In Ni-doped materials, oxygen vacancies appear to be the predominant defect, whereas in Fe-doped samples, electron holes are stabilized on Fe, leading to very different catalytic behaviour. Surface studies in combination with AA measurements reveal some dissolution of the catalyst into solution during the reaction. The surface reactivity to water is influenced by the TM d electron count, with water binding more strongly to Fe-doped materials than to those containing Ni. The influence of these factors on the rate of the unwanted hydrogen peroxide decomposition reaction and hence on activity in epoxidation is discussed.

Keywords: Aqueous epoxidation, perovskite, La₁₋ₓSrₓCoO₃, XANES, XPS.

Introduction

The electronic structure of complex transition metal oxides is of great interest, as their properties may be tailored by small changes in chemical doping level. For example, it may be possible to stabilize ions in unusually high formal oxidation states, leading to potential applications in catalysis [1].

Here we use a combination of catalytic testing with VUV photoemission and EXAFS/XANES to explore the variation in surface reactivity of the mixed cobaltates $La_{1-x}Sr_xCo_{1-y}TM_yO_3$ (TM=Ni,Fe) in aqueous solution. Our interest here lies in the possible use of these materials as heterogeneous catalysts for aqueous oxidations of organic molecules (for example epoxidation of crotyl alcohol) using hydrogen peroxide, H_2O_2, as oxidant. $LaCoO_3$ is an insulator at low temperature, but replacing La with Sr is effectively hole doping, and results in a metal-to-non-metal transition at x=0.2, with the creation of Co^{4+} ions [2]. Compensating oxygen vacancies are formed at higher concentrations, although the balance between Co^{4+} (electron hole) and oxygen vacancy creation has been a matter of some debate [2-4]. Here we explore the influence of doping the adjacent transition metals, Ni and Fe onto the Co sites in the perovskite, and study the influence this has on catalytic activity and surface reactivity.

Experimental

Ceramic samples of $La_{1-x}Sr_xCo_{1-y}TM_yO_3$ (TM=Fe, Ni) were synthesised having y = 0, 0.2,0.4,1.0 and x = 0, 0.2. Stoichiometric amounts of La_2O_3 (99.9%), $SrCO_3$(99.994%), CoC_2O_4 (and/or the respective Ni and Fe oxalates, all >99.99%) were ground together and annealed in air at 800°C for 24 hours, reground, and then heated further at 1000°C for 96 hours. After a further regrinding, the last annealing cycle was repeated. X-ray diffraction showed in general that only the perovskite ABO_3 phase was present, with a rhombohedral distortion which decreased with Sr doping level. For x=0, y=0.4 Fe, a mixed-phase rhombohedral and orthorhombic structure was formed, consistent with literature results [5]. As might be expected from the high anealing temperatures used to synthesize these 'model catalysts', the samples were highly crystalline, as evidenced by the narrow reflections observed in XRD. Consistent with this, the BET surface areas of such ceramics are much lower than in a normal working catalyst material, typically around 0.5 m^2 g^{-1}, with small random fluctuations with doping level. These are insufficiently large to affect the catalytic trends presented below (e.g. Table 2).

The activity of the samples in the decomposition of H_2O_2 was tested by measuring the volume of gas evolved from static reaction at 40 °C using a burette, as the peroxide decomposed to water and O_2. Production of epoxide from crotyl alcohol over the catalyst in aqueous solution in the presence of H_2O_2 was measured using a flow reactor connected to a gas chromatography (GC) instrument (Perkin Elmer), calibrated using $DMSO_2$. A 2M solution of epoxide with excess hydrogen peroxide was used, at a flow speed of 1 ml min^{-1} and a temperature of 40 °C. Atomic absorption (AA) spectroscopy using a Thermo Jarrell Ash Video 22E instrument was used to determine the metal content in the solutions following reaction. Photoemission and X-ray absorption measurements were carried out at the SRS, CLRC Daresbury Laboratory. Photoemission measurements used the spherical grating monochromator (15=hv=220 eV) on Station 4.1, with a Scienta 200 mm hemispherical analyzer. The position of the Fermi edge was determined by reference to the Mo sample holder. The surfaces of ceramic pellets of the catalysts were cleaned for UHV measurements by scraping using a diamond file in vacua of 5 x

$10^{-11} - 10^{-10}$ torr. In order to investigate stability in water, a series of experiments were conducted in which the surfaces were dosed with freeze-degassed doubly-distilled water. This was admitted to the vacuum chamber via a leak valve, with the exposure in langmuirs (1 L = 10^{-6} torr s) estimated from the chamber ion gauge. The samples were initially cooled to around 125 K before dosing and then warmed to room temperature. Spectra were recorded at intervals during this process. X-ray Absorption Near-edge Structure (XANES) measurements were made in transmission mode at the Fe K, Ni K and Co K-edges, using the order sorting double crystal Si (111) monochromator (4=hv=13 keV) on station 7.1. XPS data were collected using the Scienta ESCA 300 system at the RUSTI facility (CLRC Daresbury Laboratory), which incorporates a monochromated Al K α source.

## Results

Water adsorption studied by photoemission

Figure 1 shows an example of a valence band spectrum (for scraped $La_{0.8}Sr_{0.2}Co_{0.6}Fe_{0.4}O_3$, recorded at hv = 68 eV) before and after dosing with water at low temperature. The difference spectrum (dosed surface - undosed surface) is also shown. In the undosed spectrum, the binding energy region from 0 - 13 eV binding energy contains the contributions from the Co and Fe 3d and O 2p valence band states [1-6].
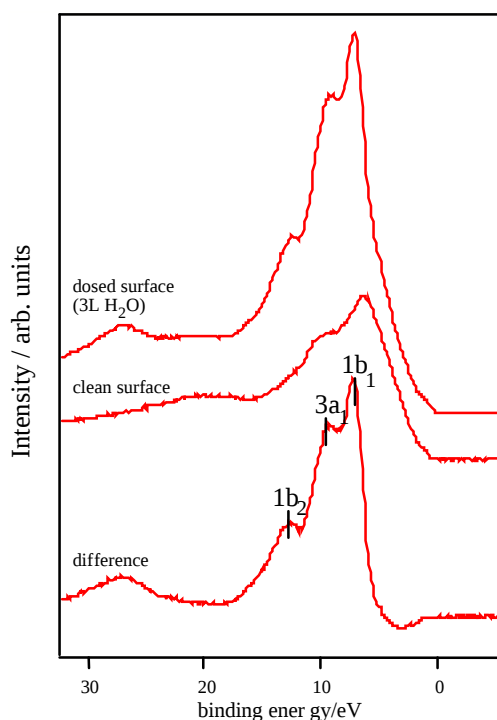
Figure 1. Valence band spectra (hv = 68 eV) of scraped and water-dosed surfaces of $La_{0.8}Sr_{0.2}Co_{0.6}Fe_{0.4}O_3$, together with the resulting difference spectrum (dosed surface - undosed surface).

Substantial changes are observed on dosing, due to the molecular orbital structure of the adsorbed water. Figure 2 shows a typical set of difference spectra (this time for a Ni-doped sample, $La_{0.8}Sr_{0.2}Co_{0.8}Ni_{0.2}O_3$, at hv = 68 eV) recorded as the sample temperature is raised following dosing. At

low temperatures, a characteristic signal of molecularly adsorbed water (three peaks) is observed, and assigned to the $1b_1$, $3a_1$ and $1b_2$ orbitals of water, together with a small feature at around 27 eV binding energy due to the O 2s core level signal also from the adsorbed water. The peak separations of the water orbitals, Δ ($3a_1$-$1b_1$) of 1.8 eV and Δ ($1b_2$ - $3a_1$) of 3.7 eV are initially quite similar to those of gas phase water (2.1 eV and 3.8 eV respectively [7]), but as the temperature is raised to 143 K, the $3a_1$ level moves to higher binding energy, giving a peak separation Δ ($3a_1$-$1b_1$) of 2.4 eV. This is typical of chemisorbed water [1], and is due to the bonding stabilization of the $3a_1$ orbital caused by its interaction with the surface. As the sample temperature is raised further, the three peaks due to water are replaced by two due to the 1π and 3σ orbitals of OH, i.e. the water dissociates. Again, this is typical behaviour for oxides of this type [1,8].
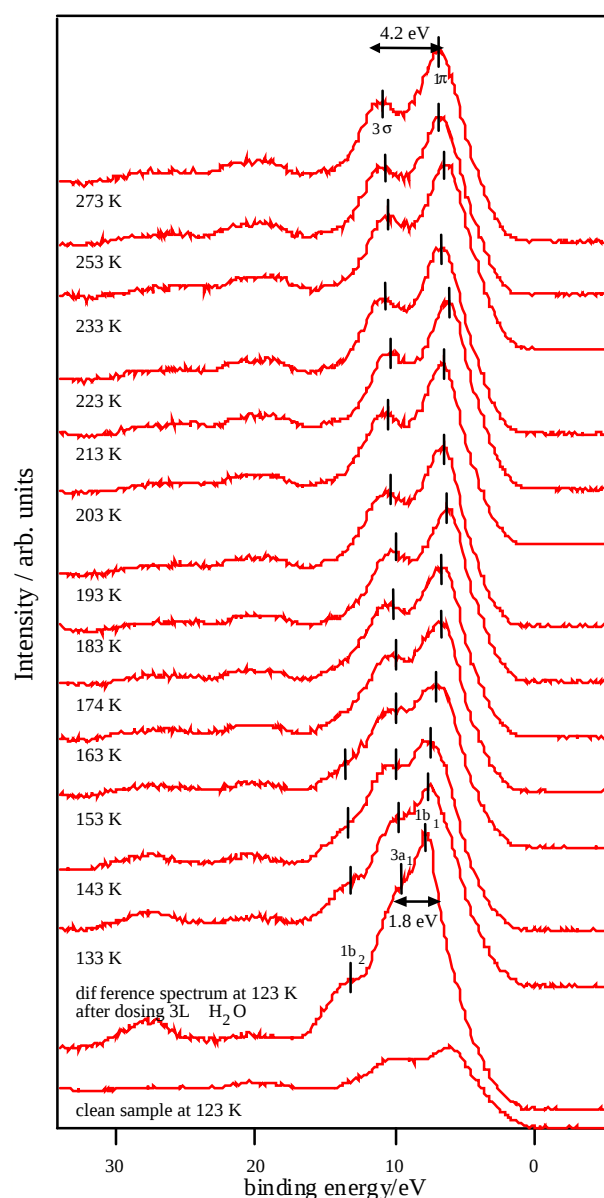
Figure 2. Clean sample spectrum and difference photoemission spectra for $La_{0.8}Sr_{0.2}Co_{0.8}Ni_{0.2}O_3$, as a function of increasing temperature after dosing with water.

The magnitude of Δ ($3a_1$-$1b_1$) varies with sample composition. Values of Δ are shown in Table 1 for the range of samples studied. It was not possible to record data at good signal-to-noise ratio for all

samples, and the figures given in Table 1 represent those obtained where the signal-to-noise ratio was at least as good as in Figure 2, allowing the value of Δ to be extracted reliably. Taking into account the possible error, it appears that water is quite strongly chemisorbed to Fe-containing samples (large Δ), but shows a less strong interaction, similar to physisorption, with Ni-doped samples. The effect of Sr doping, however, is unclear.

Table 1. Energy separation between the $1b_1$ and $3 a_1$ peaks of adsorbed water at *ca.* 125 K for a range of samples.

| sample	$\Delta (1b_1\text{-}3a_1)\pm 0.4$ eV
$LaCo_{0.8}Fe_{0.2}O_3$	2.8
$LaCo_{0.6}Fe_{0.4}O_3$	2.6
$La_{0.8}Sr_{0.2}Co_{0.6}Fe_{0.4}O_3$	2.1
$La_{0.8}Sr_{0.2}Co_{0.8}Ni_{0.2}O_3$	1.8
$LaCo_{0.6}Ni_{0.4}O_3$	1.7

Defect Structure studied by XANES

XANES at the Fe K, Co K and Ni K edges was used to study the bulk defect structures of the materials in order to elucidate any marked differences in defect chemistry between the Fe- and Ni-doped samples.
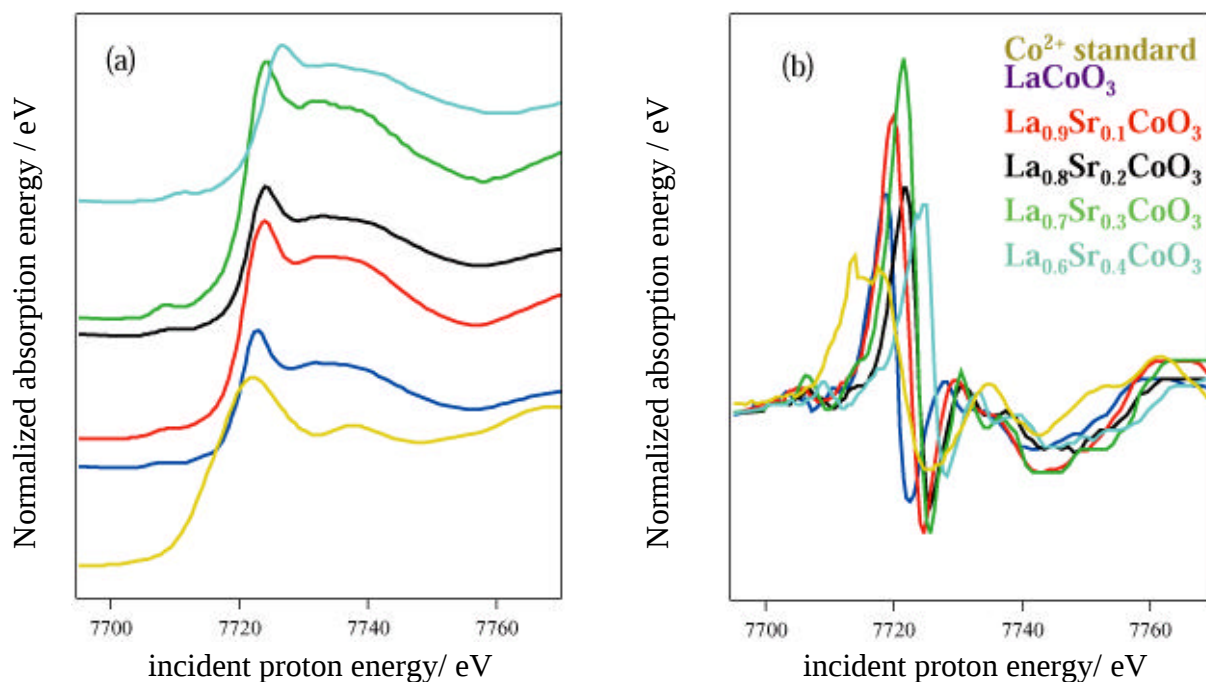
Figure 3. Normalized XANES (a) and normalized differential XANES (b) at the Co K-edge for a Co^{2+} standard (CoO), $LaCoO_3$ and $La_{1-x}Sr_xCoO_3$ (x = 0.1 – 0.4).

Figure 3 shows an example of the XANES and the differential XANES at the Co K-edge for $La_{1-x}Sr_xCoO_3$, as x is increased from 0 to 0.4. All the main absorption edges (due to the 1s → 4p transi-

tion) lie to the high photon energy side of the Co^{2+} standard, as expected, as Co in $LaCoO_3$ is in the +3 oxidation state. A small prepeak due to the dipole forbidden 1s $\rightarrow$ 3d transition is observed at around 7710 eV. As Sr is doped into the material a progressive shift of the absorption edges to higher photon energy is observed (seen most clearly in the maxima of the differential XANES spectra). This indicates a progressive increase in the valence state of Co (i.e. increased hole doping) as Sr is doped into the material up to x=0.4. This confirms that hole doping (rather than solely compensation by oxygen vacancy creation) persists to rather high Sr concentrations, consistent with the work of Nakamura *et al.* [2] and Petrov *et al.* [4].
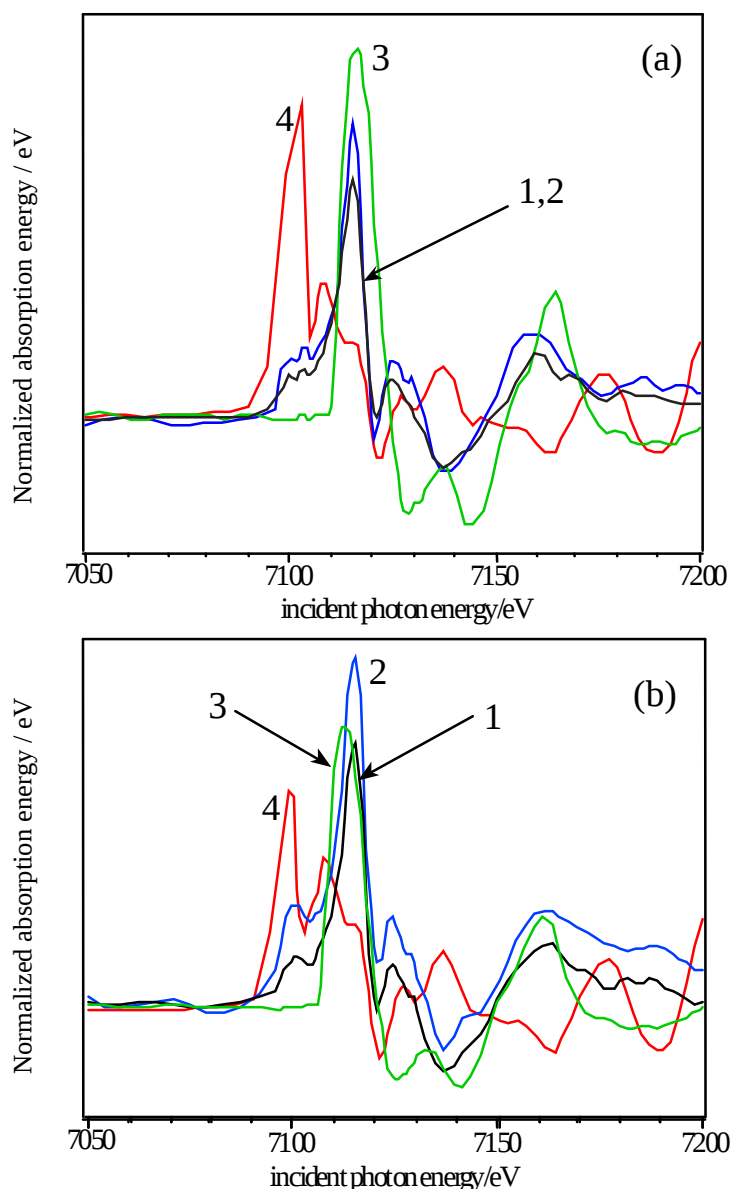

Figure 4. Normalized differential XANES structure at the Fe K-edge of 1: y=0.2 (black); 2: y=0.4(blue); 3: an Fe^{3+} standard (Fe_2O_3, green) and 4: Fe metal (red) for (a) $LaCo_{1-y}Fe_yO_3$ and (b) $La_{1-x}Sr_xCo_{1-y}Fe_yO_3$.

Figure 4 shows an example of the differential XANES at the Fe K-edge for $LaCo_{1-y}Fe_yO_3$ samples (a) and corresponding strontium-doped equivalents, $La_{1-x}Sr_xCo_{1-y}Fe_yO_3$ (b). In Fe-doped materials containing no Sr, the Fe valency appears similar to the Fe^{3+} standard. However, Sr substitution for La clearly leads to an increase in the Fe valency above 3.0, as revealed by the shift to higher binding en-

ergy (relative to the Fe^{3+} standard) of the normalized differential XANES structures for Sr-doped samples 1 and 2 shown in Figure 4(b). Data obtained at the corresponding Co K-edge for these samples show no increase in the Co oxidation state on Sr-subsitution [9] i.e. electron holes are stabilized on Fe (rather than on Co) in $La_{1-x}Sr_xCo_{1-y}Fe_yO_3$, leading to Fe^{4+}, rather than Co^{4+}, consistent with the findings of Tai *et al.* [5]. This effect is not observed in samples doped with Ni, where on Sr substitution, no increase is seen in either the Ni or Co oxidation states [9]. We therefore speculate that the defect chemistry in $La_{1-x}Sr_xCo_{1-y}Ni_yO_3$ is controlled largely by compensating oxygen vacancies, a suggestion supported by the low coordination numbers to O observed in corresponding EXAFS measurements [9].

Catalytic measurements

The results of a typical reaction study for an active (i.e. epoxide-producing) catalyst are shown in Figure 5.
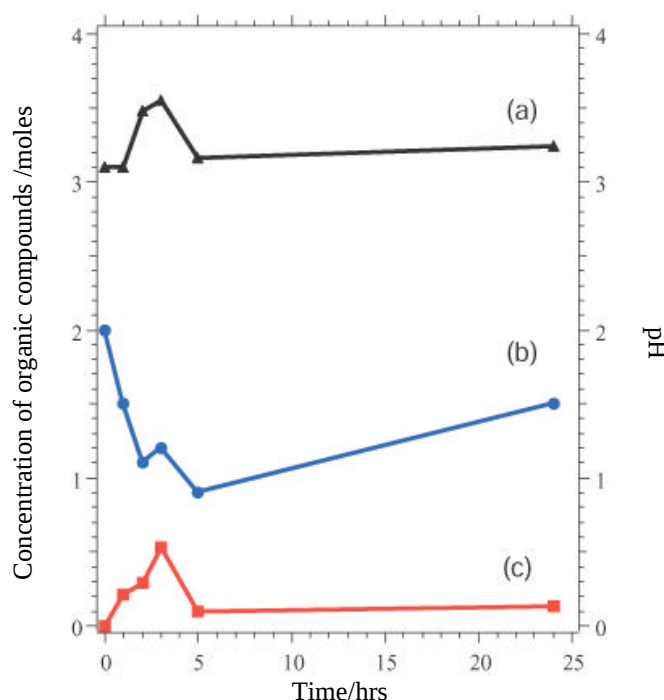
Figure 5. The pattern of catalytic activity and changes in pH as a function of time for $La_{0.8}Sr_{0.2}Co_{0.6}Ni_{0.4}O_3$; (a) pH during the reaction; (b) crotyl alcohol (reactant) concentration; (c) epoxide (product) concentration.

This pattern of reaction (i.e. epoxide production over the first 5 hours, in some cases with an induction period, together with an apparent pH dependence) was observed in general for all active samples. The most active epoxide producing catalysts were found to be those containing Co, or Co/Ni, with or without Sr, with Fe-containing samples showing rather less activity (Table 2). This again highlights a strong difference between Fe-containing samples and those containing no Fe, reinforcing the contrast between these samples observed in both the adsorption studies and the XANES measurements. The rates of hydrogen peroxide decomposition were also measured via the volume of oxygen evolved in separate experiments. The results for a typical set of samples (having x=0.2) are summarized in Table 2. It can be seen that the low activity of the Fe and Fe/Sr samples in epoxide production correlates with their high activity in peroxide decomposition, i.e. the Fe-containing samples are inactive in ep-

oxidation at least in part because they are very effective in the breakdown of the oxidant, hydrogen peroxide.

Throughout the flow reactions, the amounts of metal ions in solution were monitored using atomic absorption (AA) spectroscopy. Leaching of all the metals into solution was detected, and this appeared to be particularly marked in the case of La and Co. Moreover, maximum leaching of the transition metals was found to occur at times of maximum activity, as shown in Figure 6.

Table 2: Summary of catalysis data for a sample set with x=0.2. The 2nd and 3rd columns refer to the maximum concentration of epoxide and the total epoxide amount produced during a 24 hour flow reaction under the conditions specified in section 2. The final column indicates the rate of oxygen production in the decomposition of peroxide over the same catalysts in a static reactor also at 40°C.

| sample	[epoxide]$_{max}$ (moles)	Total epoxide (moles)	d[O$_2$]/dt/ ml g^{-1} h^{-1}
La$_{0.8}$Sr$_{0.2}$CoO$_3$	0.80	0.80	15.14
La$_{0.8}$Sr$_{0.2}$Co$_{0.8}$Fe$_{0.2}$O$_3$	0.00	0.00	33.11
La$_{0.8}$Sr$_{0.2}$Co$_{0.6}$Fe$_{0.4}$O$_3$	0.14	0.52	44.67
La$_{0.8}$Sr$_{0.2}$Co$_{0.8}$Ni$_{0.2}$O$_3$	0.02	0.08	15.85
La$_{0.8}$Sr$_{0.2}$Co$_{0.6}$Ni$_{0.4}$O$_3$	0.53	1.05	14.13
Blank (no sample)	0.02	0.02	0.02
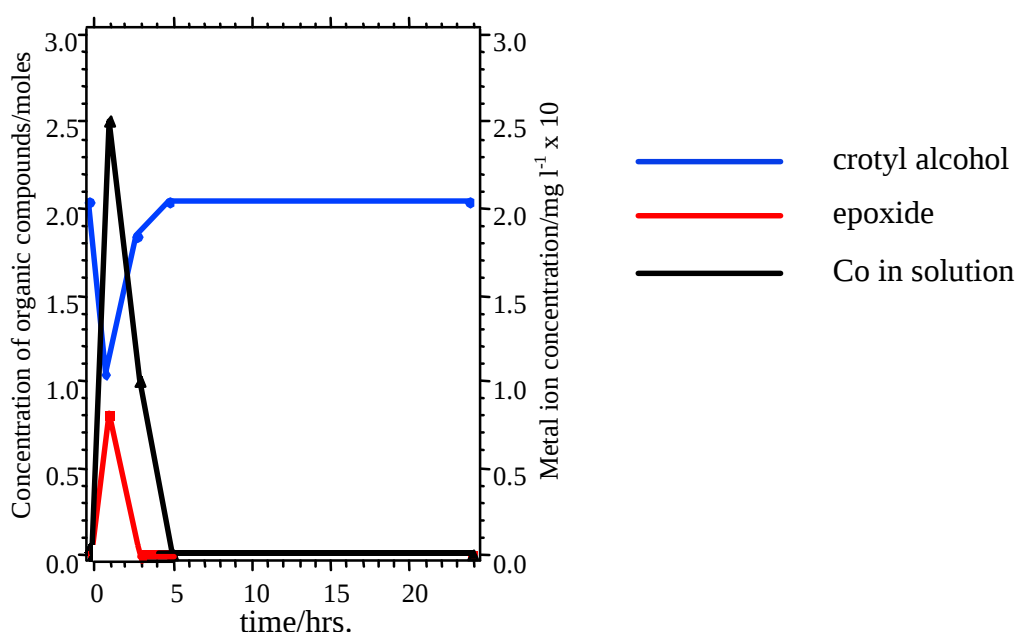
Figure 6. The leaching of Co into solution during catalytic reaction over La$_{0.8}$Sr$_{0.2}$CoO$_3$ as measured by AA. Corresponding GC measurements of the concentrations of epoxide and crotyl alcohol are also shown.

However, further GC measurements using solutions of the transition metal ions mixed with the reactor feedstock solutions showed no epoxide production, suggesting that epoxidation is not occurring by homogeneous reaction in aqueous solution [9]. Catalyst re-use tests showed that materials which were initially active remained active following an initial catalytic cycle, although often with a lengthened induction period. These results suggest some dissolution of the catalyst in the highly acidic feedstock solution. These conclusions are reinforced by the marked drop in the amount of epoxide produced with time (after around 3-5 hours), which can be seen in both Figures 5 and 6. This suggests that there is some change occurring at the surface of the catalyst during the reaction cycle that affects its ability to produce epoxide, for example dissolution of the catalytically active species into the feedstock solution.

XPS measurements

In order to explore further the possible dissolution of the catalyst during reaction, XPS measurements of the surface composition were made from as-presented catalyst samples, and from samples following catalytic reaction. The reacted catalysts were removed from solution at the point of maximum epoxide production. An example of the Co 2p spectra obtained is shown in Figure 7, with corresponding elemental quantification in Table 3.
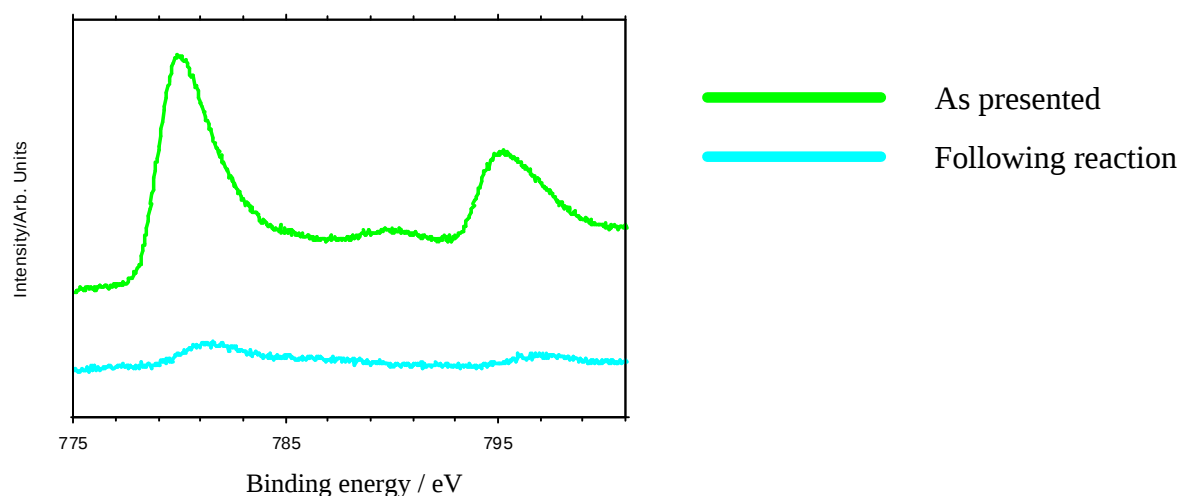
Figure 7. Co $2p_{3/2,1/2}$ peaks for $La_{0.8}Sr_{0.2}CoO_3$ in the as-presented state and following catalytic reaction.

In general the peak shapes observed for the 'as-presented' samples are complex, and indicative of a perovskite surface contaminated with a series of degradation products which may include $La(OH)_3$ and $SrCO_3$ (as strong high-binding energy features are observed in the Sr 3d, and O 1s spectra, two separate sets of $4f^0\underline{L}^0$ and $4f^1\underline{L}^1$ features are observed in the La 3d spectra, and a carbonate feature is observed in some of the C 1s spectra [9]). These features are typical of RE/TM perovskites and layered perovskites which have been exposed to atmospheric H_2O and CO_2, and have been discussed elsewhere [1]. Quantification of the chemical composition of these surfaces generally reveals surfaces which are slightly enriched in La relative to the bulk nominal composition, but strongly deficient in transition metals. Examples are given in Table 3.

Following catalytic reaction, marked changes in composition are observed, with samples typically showing a significant reduction in surface La content, a small increase in C and O content, and the presence of some surface Sn (used as a stabilizer in the H_2O_2 feedstock solution). However, the most significant change is a very large reduction in surface TM content, illustrated for the case of Co in Figure 7 and Table 3. The increase in C and O content is expected following reaction and may be caused by the residual adsorption of reactants and products at the surface. This may slightly attenuate the underlying metal signals from the catalyst. It does not, however, explain the very significant change in the La:TM ratio after reaction, which provides further evidence for leaching of transition metals from the catalyst into solution during the reaction.

Table 3: Ratios of the elements present at the surface of $La_{1-x}Sr_xCoO_3$ samples before and after catalytic reaction, as determined by XPS. The data are normalized to [La]+[Sr]+[Co]+[O] = 5 for direct comparison with the nominal bulk composition (also shown).

x	La	Sr	Co	O	C	Sn
0 - nominal composition	1	-	1	3	-	-
0 - as presented	1.23	-	0.28	3.48	0.67	-
0 - following reaction	0.85	-	0.07	4.08	0.75	0.11
0.2 - nominal composition	0.8	0.2	1	3	-	-
0.2 - as presented	0.83	0.26	0.50	3.41	0.98	-
0.2 - following reaction	0.61	0.43	0.04	3.92	1.13	0.15

Discussion

Adsorption studies indicate that the ability of these surfaces to chemisorb water changes with transition metal content. This may be associated with the changing d-electron count of the cations as Co is replaced by Ni or Fe. In cases of strong chemisorption, the interaction between water and transition metal cations on oxide surfaces is of a donor-acceptor type, typically with direct donation from the filled $3a_1$ orbital of water into any empty metal 3d levels of the correct symmetry (for an octahedrally coordinated ion, dz^2, e_g). This leads to a bonding stabilisation of the donor levels, and an antibonding destabilisation of the acceptor metal d level [10]. In the Co containing samples, Co^{3+} (d^6) exists in either a high spin (HS) or (predominantly) in an intermediate spin (IS) state [6], with only partial occupancy of the e_g levels (which are further depopulated on Sr doping, forming some Co^{4+}). In the Fe-containing samples, the d electron count is lowered, and XANES indicates that the Fe valency in the absence of Sr is Fe^{3+} (d^5), with some Fe^{4+} (d^4) formed on Sr-doping. In contrast, for Ni containing samples, EXAFS indicates a bondlength intermediate between that of Ni^{2+}-O and Ni^{3+}-O, i.e. a raised d electron count of between d^8 and d^7 [9], and XANES indicates that this does not change on Sr-doping. We may expect that at the surface where adsorption occurs, the regular octahedral coordination of the

transition metal ions is broken by the surface, and indeed, cluster calculations by Kojima *et al.* [11] for LaCoO$_3$ and LaFeO$_3$ indicate that stable clusters of the type $(TMO_5)^{7-}$ exist. This raises the degeneracy of both the t$_{2g}$ and the e$_g$ levels. Of particular interest here is the prediction that Fe^{3+} (d^5) exists at the surface not as HS but in a low spin (LS) state with an unoccupied d$_z{}^2$ orbital [12], which would lead to a large donor-acceptor interaction on binding water. This is illustrated in Figure 8 [12]. In contrast Ni^{2+} (LS) has a filled d$_z{}^2$ level, and thus water might be expected to be essentially physisorbed, as is observed. Overall, we would therefore expect water to bind less strongly to Ni-containing samples than to those containing Fe, and this appears to be borne out by the data contained in Table 1. We have noted in earlier work that replacing Co by Cu in these systems also results in a decrease in the surface reactivity with water [13].
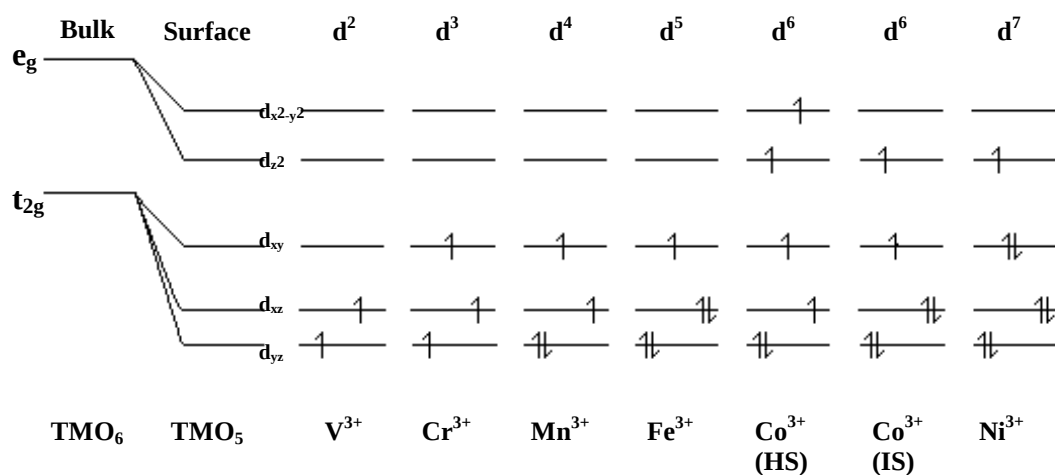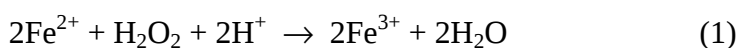

Figure 8. d electron configurations for surface TM^{3+} ions, adapted from reference 12.
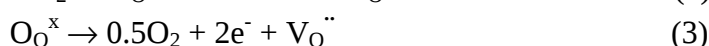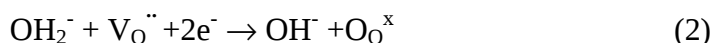
The catalysis results indicate that the Fe-containing materials decompose peroxide at a substantially higher rate than those containing Ni/Co or Co. The strong reaction between water and Fe-containing samples may aid the leaching of Fe into solution during the reaction, which as the reaction medium is strongly acidic, would exist in solution as Fe^{2+} [14]. Iron in a divalent state is known to readily decompose peroxide under acidic conditions via a Fenton type reaction [15,16]:

$$2Fe^{2+} + H_2O_2 + 2H^+ \rightarrow 2Fe^{3+} + 2H_2O \qquad\qquad (1)$$

XPS and AA give clear evidence for leaching of transition metals into solution during reaction. Thus, the increased reactivity of Fe-containing catalysts to water may promote homogeneous decomposition of the oxidant, hydrogen peroxide, and lead to a decrease in activity in epoxidation, as seen in Table 2.

We may expect any heterogeneous mechanisms for the decomposition of peroxide to be influenced by the bulk defect chemistry, and here XANES indicates that there are marked differences between Fe-doped and Ni-doped samples. Hole doping Fe-containing materials leads to production of Fe^{4+}. In contrast, in LaCo$_{1-y}$Ni$_y$O$_3$, EXAFS and XANES indicate that Ni is present as mixed Ni^{2+} and Ni^{3+} [9]. On hole-doping with Sr, the introduced holes appear to be compensated by the creation of oxygen vacancies [9] and some Ni^{2+} remains. These results are consistent with those of Rajeev *et al.* for this

phase [17]. TPD studies of these perovskites have indicated the presence of two types of oxygen, α-oxygen and β-oxygen [18]. The former desorbs at low temperatures ($< 300°C$) and is associated with loosely-bound absorbed oxygen accommodated in oxygen vacancy sites in the lattice [18], and implicated in catalytic activity. Studies of $La_{1-x}Sr_xCo_{1-y}Fe_yO_3$ [19,20] have shown that the amount of α-oxygen increases on Sr-doping, stabilizing the Fe^{4+} created on hole doping. In contrast, the amount of α-oxygen in Ni-doped catalysts is relatively low [20], consistent with the XANES measurements. A large supply of such oxygen is important to heterogeneous peroxide decomposition, thought to occur via a two-step mechanism proposed by Zhang [19]:

$$OH_2^- + V_O^{\cdot\cdot} + 2e^- \rightarrow OH^- + O_O^x \qquad (2)$$
$$O_O^x \rightarrow 0.5O_2 + 2e^- + V_O^{\cdot\cdot} \qquad (3)$$

Heterogeneous peroxide decomposition is therefore favoured in Fe-containing samples. Thus, both homogeneous and heterogeneous pathways to the unwanted peroxide decomposition reaction are favoured over Fe-containing samples. In contrast, we expect the desired epoxidation reaction to be favoured in the Ni- and Co-containing materials. In general, epoxidation by late transition metals is via the production of a nucleophilic epoxide species, HO_2^-, and attack of this species on the double bond of the organic starting compound [21] bound to the surface. While our studies give us no information about the binding site of the crotyl alcohol on the surface, the work of Voorhoeve has shown that oxidation over perovskites of the type studied here occurs most efficiently at transition metal ions having quite full t_{2g} levels and one or no e_g electrons [22]. This maximises any synergic bonding between the TM site and unsaturated bonds in the organic starting compound. The most suitable configurations in our case are likely to be Ni^{3+} and IS Co^{3+} (Figure 8). Thus catalysts containing Co and Co/Ni are efficient epoxidation catalysts, and are also relatively inefficient in unwanted peroxide decomposition.

Nevertheless, these materials do show properties which are ultimately undesirable in a working catalyst. GC measurements indicate that there is an initial induction period before reaction begins, while XPS shows that the as-presented catalyst surfaces are initially rich in La-containing contaminant phases. The dissolution of these phases in the highly acidic reaction medium, producing La^{3+} in solution may be one factor leading to the increase in pH seen in the initial reaction stages (Figure 5). The induction period may be associated with the stripping of these phases from the surface to expose the active TM sites. When reaction does commence, marked leaching of the TM ions into solution is observed (Figure 6), which is undesirable in a working material, and leads to a reduction in the rate of epoxide production typically 3-5 hours into the catalytic reaction. XPS data taken following reaction reveal a marked reduction in surface TM. Reuse tests on these materials show that initially active catalysts retain their activity on reuse, but often with a lengthened induction period before epoxide production begins. This may be because the surface layers of the catalyst, previously depleted in TM, must be stripped before TM-rich layers of the catalyst are again exposed.

Conclusions

SR photoemission and XANES reveal marked differences in surface and bulk defect chemistry between Fe-substituted and Ni-substituted catalysts which correlate with variations in catalytic activity. Adsorption studies indicate that Fe-doped materials chemisorb water more strongly than Ni-substituted

counterparts, which may raise the rate of unwanted homogenous decomposition of the peroxide oxidant in the catalytic medium. XANES indicates that in Fe-doped materials, holes are stabilized on Fe, whereas in Ni-doped materials, oxygen vacancy compensation is the predominant mechanism. This influences the proportion of α-oxygen present in the materials, and acts to raise the rate of heterogeneous peroxide decomposition in the Fe-substituted materials. Both heterogeneous and homogenous pathways contribute to a raised level of unwanted peroxide decomposition over Fe-substitued materials, leading to a reduced efficiency in the desired epoxidation reaction. In contrast, catalysts containing Co only and Co/Ni are efficient epoxidation catalysts, and are also relatively inefficient in unwanted peroxide decomposition. Leaching of all transition metal ions into solution is observed during catalytic reaction, and this would need to be addressed before these materials could be used as working catalysts.

Acknowledgments

References

1. Howlett, J.F.; Flavell, W.R.; Thomas, A.G.; Hollingworth, J.; Warren, S.; Hashim, Z.; Mian, M.; Squire, S.; Aghabozorg, H.R.; Sarker, Md. M.; Wincott, P.L.; Teehan, D.; Downes, S.; Law, D.S.-L.; Hancock, F.E. *Faraday Discuss.* **1996**, *105*, 337.
2. Nakamura, T.; Misono, M.;Yoneda, Y. *J Catal.*, **1983**, *83*, 151.
3. Jonker, G.H.; van Santen, J.H. *Physica*, **1953**, *19* , 120.
4. Petrov, A.N.; Konochuk, O.N.; Andreev, A.V.; Cherepanov, A.V.; Kofstad, P. *Solid State Ionics*, **1995**, *80*, 189.
5. Tai, L.W.; Nasrallah, M.M.; Anderson, H.U.; Sparlin, D.M.; Sehlin, S.R.; *Solid State Ionics*, **1995**, *76*, 273.
6. Thomas, A.G.; Flavell, W.R.; Dunwoody, P.M.; Mitchell, C.E.J.; Warren, S.; Grice, S.C.; Marr, P.G.D.; Jewitt, D.E.; Khan, N.; Downes, S.W.; Teehan, D.; Seddon, E.A.; Asai, Kichizo; Kobayashi, Yoshihiko; Yamada, Nobuyoshi *J. Phys. Condens. Matter,* **2000**, *12,* 9259.
7. Siegbahn, K. *J. Electron Spectrosc. Relat. Phenom.,* **1974**, *5*, 1.
8. Kurtz, R.L.; Stockbauer, R.; Madey, T.E.; Mueller, D.; Shih, A.; Toth, L. *Phys. Rev. B*, **1988**, *37*, 7936.
9. Grice, S.C. *PhD Thesis*, UMIST, **2000**; in preparation for publication.
10. Henrich, V.E.; Cox, P.A. *The Surface Science of Metal Oxides*, Cambridge University Press, Cambridge, **1994**, p. 258.
11. Kojima, I.; Adachi, H.; Yasumari, I. *Surf. Sci.,* **1983**, *130*, 50.
12. Fierro, J.L.; Tejuca, L.G. *Properties and Applications of Perovskite-type Oxides*, Marcel Dekker, New York, **1993**.
13. Hollingworth, J.; Flavell, W.R.; Thomas, A.G.; Grice, S.C.; Mitchell, C.E.J.; Dunwoody, P.M.; Warren, S.; Squire, S.J.; Marr, P.G.D.; Downes, S.W.; Hancock, F.E.; *J. Electron Spectrosc. Relat. Phenom.,* **1999**, *101-103*, 765.
14. Pourbaix, M. *Memoires Soc. Roy. Belge Ingenieurs et Industriels*, **1951**,*1*, 1.
15. Tang, W.Z.; Huang, P.C. *Env. Tech.,* **1996**, *17*, 1371.

16.   Tang, W.Z.; Huang, P.C. *Env. Tech.,* **1997**, *18*, 13.

17.   Rajeev, K.P.; Raychaudhari, A.K. *Phys. Rev. B*, **1992**, *46*, 1309.

18.   Teraoka, Y.; Zhang, H.M.; Yamazoe, N. *Chem. Lett.,* **1985**, 1367.

19.   Zhang, H.M.; Shimizu, Y.; Teraoke, Y., Miura, N.; Yamazoe, N. *J. Catal.,* **1990**, *121*, 432.

20.   Zhang, H.M.; Yamozoe, N.; Teraoka, Y. *J. Mat. Sci. Lett.,* **1989**, *8*, 995.

21.   Strukul, G (ed.) *Catalytic Oxidations with Hydrogen Peroxide as Oxidant,* Kluwer Academic Publishers, Dordrecht, **1992**.

22.   Voorhoeve, R.J.H. in *Advanced Materials in Catalysis* ed. Burton, J.L.; Garten, R.L., *Mater. Sci. Series*, Academic Press, New York, **1977**.